REPORT DOCUMENTATION PAGE

Form Approved
OMB No. 0704-0188

PLEASE DO NOT RETURN YOUR FORM TO THE ABOVE ORGANIZATION.

1. REPORT DATE *(DD-MM-YYYY)*	2. REPORT TYPE	3. DATES COVERED *(From - To)*
28-08-2012	Final	01-08-2009 - 31-07-2012

4. TITLE AND SUBTITLE
High Power Optical Coatings by Atomic Layer Deposition and Signatures of Laser-Induced Damage

5a. CONTRACT NUMBER

5b. GRANT NUMBER
N00014-09-1-1112

5c. PROGRAM ELEMENT NUMBER

6. AUTHOR(S)
Joseph J. Talghader - University of Minnesota - joey@umn.edu

5d. PROJECT NUMBER

5e. TASK NUMBER

5f. WORK UNIT NUMBER

7. PERFORMING ORGANIZATION NAME(S) AND ADDRESS(ES)
University of Minnesota, Office of Sponsored Projects Administration
200 Oak St. SE, Suite 450
Minneapolis, MN 55455-2070

8. PERFORMING ORGANIZATION REPORT NUMBER

9. SPONSORING/MONITORING AGENCY NAME(S) AND ADDRESS(ES)
Office of Naval Research
875 North Randolph Street
Arlington, VA 22203-1995
ATTN: Quentin Saulter

10. SPONSOR/MONITOR'S ACRONYM(S)
JTO/ONR

11. SPONSOR/MONITOR'S REPORT NUMBER(S)

12. DISTRIBUTION/AVAILABILITY STATEMENT
Unlimited

13. SUPPLEMENTARY NOTES

14. ABSTRACT
This report describes an investigation of the properties of optical coating oxides deposited by atomic layer deposition. Specifically, two oxides were chosen as indicative of the group as a whole: aluminum oxide (Al2O3) and hafnium oxide (HfO2). Uniform films and nanolaminates (films with inserted layers of alternate materials) were deposited and tested for thermal conductivity, absorption, and laser damage threshold, among other properties. Significant effort went into the analysis of the thermal conductivities of the films since thermal breakdown is particularly relevant to directed energy applications. The interface thermal resistance in hafnia-alumina nanolaminates is very low and does not dominate the film thermal conductivity. The degree of crystallinity of these films appears to have a much larger effect on thermal conductivity than that of interface density. Cryogenic measurements show partial agreement with both the minimum thermal conductivity model for disordered solids and the diffuse mismatch model of interface resistance. Absorption measurements show results less than or near 1ppm, which matches or exceeds the performance of the best films deposited by other methods.

15. SUBJECT TERMS
Optical Coatings, Atomic Layer Deposition, Thermal Conductivity

16. SECURITY CLASSIFICATION OF:			17. LIMITATION OF ABSTRACT	18. NUMBER OF PAGES	19a. NAME OF RESPONSIBLE PERSON
a. REPORT	b. ABSTRACT	c. THIS PAGE			Joseph J. Talghader
U	U	U	UU	28	19b. TELEPHONE NUMBER *(Include area code)* (612) 625-4524

INSTRUCTIONS FOR COMPLETING SF 298

1. REPORT DATE. Full publication date, including day, month, if available. Must cite at least the year and be Year 2000 compliant, e.g. 30-06-1998; xx-06-1998; xx-xx-1998.

2. REPORT TYPE. State the type of report, such as final, technical, interim, memorandum, master's thesis, progress, quarterly, research, special, group study, etc.

3. DATES COVERED. Indicate the time during which the work was performed and the report was written, e.g., Jun 1997 - Jun 1998; 1-10 Jun 1996; May - Nov 1998; Nov 1998.

4. TITLE. Enter title and subtitle with volume number and part number, if applicable. On classified documents, enter the title classification in parentheses.

5a. CONTRACT NUMBER. Enter all contract numbers as they appear in the report, e.g. F33615-86-C-5169.

5b. GRANT NUMBER. Enter all grant numbers as they appear in the report, e.g. AFOSR-82-1234.

5c. PROGRAM ELEMENT NUMBER. Enter all program element numbers as they appear in the report, e.g. 61101A.

5d. PROJECT NUMBER. Enter all project numbers as they appear in the report, e.g. 1F665702D1257; ILIR.

5e. TASK NUMBER. Enter all task numbers as they appear in the report, e.g. 05; RF0330201; T4112.

5f. WORK UNIT NUMBER. Enter all work unit numbers as they appear in the report, e.g. 001; AFAPL30480105.

6. AUTHOR(S). Enter name(s) of person(s) responsible for writing the report, performing the research, or credited with the content of the report. The form of entry is the last name, first name, middle initial, and additional qualifiers separated by commas, e.g. Smith, Richard, J, Jr.

7. PERFORMING ORGANIZATION NAME(S) AND ADDRESS(ES). Self-explanatory.

8. PERFORMING ORGANIZATION REPORT NUMBER. Enter all unique alphanumeric report numbers assigned by the performing organization, e.g. BRL-1234; AFWL-TR-85-4017-Vol-21-PT-2.

9. SPONSORING/MONITORING AGENCY NAME(S) AND ADDRESS(ES). Enter the name and address of the organization(s) financially responsible for and monitoring the work.

10. SPONSOR/MONITOR'S ACRONYM(S). Enter, if available, e.g. BRL, ARDEC, NADC.

11. SPONSOR/MONITOR'S REPORT NUMBER(S). Enter report number as assigned by the sponsoring/ monitoring agency, if available, e.g. BRL-TR-829; -215.

12. DISTRIBUTION/AVAILABILITY STATEMENT. Use agency-mandated availability statements to indicate the public availability or distribution limitations of the report. If additional limitations/ restrictions or special markings are indicated, follow agency authorization procedures, e.g. RD/FRD, PROPIN, ITAR, etc. Include copyright information.

13. SUPPLEMENTARY NOTES. Enter information not included elsewhere such as: prepared in cooperation with; translation of; report supersedes; old edition number, etc.

14. ABSTRACT. A brief (approximately 200 words) factual summary of the most significant information.

15. SUBJECT TERMS. Key words or phrases identifying major concepts in the report.

16. SECURITY CLASSIFICATION. Enter security classification in accordance with security classification regulations, e.g. U, C, S, etc. If this form contains classified information, stamp classification level on the top and bottom of this page.

17. LIMITATION OF ABSTRACT. This block must be completed to assign a distribution limitation to the abstract. Enter UU (Unclassified Unlimited) or SAR (Same as Report). An entry in this block is necessary if the abstract is to be limited.

FINAL REPORT

High Power Optical Coatings by Atomic Layer Deposition and Signatures of Laser-Induced Damage

Grant #: N00014-09-1-1112
Program Period: 1 August 2009 to 31 July 2012
(one year funded)

Principal Investigator: Joseph J. Talghader
University of Minnesota
Electrical and Computer Engineering
4-174 EE/CSci Building
200 Union Street SE
Minneapolis, MN 55455
Phone: (612) 625-4524
Fax: (612) 625-4583
joey@umn.edu

This program was a single year program with options for years 2 and 3. Since the options were not contracted, this report covers work that was primarily performed between August 1, 2009 and July 31, 2010, with related publications appearing the next year. Several samples of the ALD work reported here (see particularly Section III) were later used in experiments under contract FA9451-10-D-0224.

I. Objectives and Executive Summary:

One of the most promising optical coatings technologies developed in recent years has been deposition using Atomic Layer Deposition (ALD). This technique provides very high control over the thickness of films since the growth is self-limiting. Further, it is almost completely conformal with high uniformity across the film. ALD also allows one to introduce very thin layers (often but not precisely accurately called monolayers) of one material individually into a film composed largely of different materials. These are called nanolaminates. This process allows one to interrupt the growth of crystal grains in thin films, creating amorphous films from naturally polycrystalline materials. It is generally accepted that amorphous films are better than polycrystalline ones for optical coating applications because of their lower scattering and absorption losses. However, for very high power continuous wave (CW) applications such as those seen in laser weaponry, the enhanced thermal dissipation of a polycrystalline film can be desirable as well and the trade-off between amorphous and polycrystalline can become less clear.

In this program, we have investigated the crystal structure and thermal conductivity of ALD films and nanolaminates in detail. Hafnia-alumina nanolaminates show improved smoothness and reduced crystallinity relative to pure hafnia in films formed by atomic layer deposition (ALD). However, typical nanolaminates also show reduced cross-plane thermal conductivity due to the much larger interface density relative to continuous films. We find that the interface thermal resistance in hafnia-alumina nanolaminates is very low and does not dominate the film thermal conductivity, which is 1.0 to 1.2 W/(m K) at room temperature in 100 nm thin films regardless of the interface density. Measured films had a number of interfaces ranging from 2 to 40, equivalent to interface spacing varying from about 40 to 2 nm. The degree of crystallinity of these films appears to have a much larger effect on thermal conductivity than that of interface density. Cryogenic measurements show good agreement with both the minimum thermal conductivity model for disordered solids and the diffuse mismatch model of interface resistance down to about 80 K before diverging. We find that the films are quite smooth through a 400:5 ratio of hafnia to alumina in terms of ALD cycles, and the refractive index scales as expected with increasing alumina concentration.

We have also examined the absorption and laser damage thresholds of our ALD HfO_2 and Al_2O_3 films at independent labs at Colorado State University (Carmen Menoni), the University of New Mexico (Wolfgang Rudolph), and Stanford University (Ashot Markosyan). These results of these tests show that the films have high laser damage thresholds and extremely low absorptions, the latter less than 1ppm in most regions tested.

II. Personnel:

In the single funded year of this program, the following primary personnel were supported:

Joseph Talghader – Principal Investigator – Professor – University of Minnesota

Nick Gabriel – Ph.D. Student – University of Minnesota

III. Accomplishments/New Findings:

A.) Thermal Conductivity and Crystal Structure of Atomic Layer Deposition Nanolaminates

This section is derived from the recent publication in the *Journal of Applied Physics* **110**, 043526 (2011) by the investigator and a recent Ph.D. graduate from his group, Dr. Nick Gabriel, currently at 3M Corporation.

A1. Introduction

Ultra-thin hafnium oxide films grown by atomic layer deposition (ALD) have been applied to gate dielectrics in field effect transistors [1-3], but at larger thicknesses they are partially crystalline and tend to have high surface roughness due to the variation in growth rate between crystallites and amorphous regions [4,5]. These relatively higher thicknesses, near 100 nm, are particularly relevant to optical coating applications where crystallinity and roughness are detrimental [6]. Nanolaminate films consisting of occasional layers of alumina (Al_2O_3) to form hafnia-rich coatings have been demonstrated to substantially reduce the roughness and crystallinity [4], but the upper limit in the hafnia:alumina ratio remained somewhat vague. In a study of the nanosecond-scale laser-induced damage threshold (LIDT) of an ALD titania-alumina nanolaminate relative to a polycrystalline titania film indicated that the smooth, amorophous nanolaminate had at least twice the LIDT of the titania film [6].

A serious potential trade-off that has been demonstrated in similar nanolaminates is reduced thermal conductivity due to the high interface density that scatters phonons [7]. While the reduced thermal conductivity is advantageous for thermal barrier coatings and thermoelectric materials, it can be detrimental to the performance of optical coatings, particularly in high-power laser systems.

We set out to characterize the thermal conductivity of these hafnia-based nanolaminates and also investigate the variation in refractive index, surface roughness, and crystallinity due to hafnia concentration above the 100:5 hafnia:alumina upper limit suggested by Hausmann and Gordon [4]. Maximizing the hafnia content should lead to larger effective refractive index and the smaller interface density to increased thermal conductivity, both advantages for optical coatings.

The differential 3ω method is applied to measure the thermal conductivity of each thin film [8,9]. The method is derived from the original 3ω technique that was applied to bulk materials based on the frequency-dependent third-harmonic response of a heater wire deposited on a substrate [10]. It was later extended to measurements of dielectric

films using the frequency-independent offset introduced by a thin film [11]. The thin-film technique required calculation of a substrate model for direct comparison to the measured data, which is sensitive to errors in assumed substrate thermal properties, particularly the heat capacity, that can introduce an offset in the model indistinguishable from the thin film contribution.

That original thin-film 3ω technique has a lower limit of about 200 nm in practice [11,12]. In contrast, the differential 3ω method compares a particular multilayer film to a reference film where the layer of interest is omitted, eliminating the need to apply handbook values for substrate properties. The potential trade-off is that the differential result contains the uncertainty from two experimental measurements rather than one, but in practical cases with careful measurements this tends to be less than the combined uncertainty [8] in substrate thermal conductivity, heat capacity, and a geometrical factor usually referred to as η, especially when measuring very thin films or over a wide temperature range.

A2. Experimental

Thin films containing alumina and hafnia were grown by atomic layer deposition in a commercial reactor at 250°C. Alumina was formed from alternating pulses of water and trimethylaluminum (TMA), and hafnia from pulses of water and tetrakis(dimethylamido) hafnium (TDMAH) with the latter held at 75°C to maintain adequate vapor pressure [13]. There have been a variety of other precursor materials investigated for ALD of hafnia, but the alkylamide-based chemicals, particularly TDMAH, have shown desirable growth and film properties [14]. Both processes yield 0.1 nm per alternating cycle, providing a means for precise control of layer thickness. To reduce roughness and crystallinity, hafnia-rich nanolaminates with a varying periodic thickness of hafnia were grown by systematically changing the number of alternating-pulse growth cycles, based on the work of Hausmann and Gordon [4]. All films were deposited on pieces from B-doped, 1–10 Ω-cm, 100 mm diameter (100) silicon wafers.

Table I – Parameters of the nanolaminates studied in this work.

Shorthand[b]	Hafnia cycles per period	Number of periods	Interface spacing[a] (nm)
NL400	400	2.25[c]	40.0
NL200	200	4.5	20.0
NL100	100	10.5	10.0
NL50	50	20.5	5.0
NL20	20	40.5	2.0

[a]Interface spacing is given as the thickness of the hafnia layers based on 0.10 nm/cycle, which is one possible interpretation of the spacing between interfaces.

[b]Used to refer to a particular design in figures and text.

[c]To maintain overall thickness near 100 nm, this structure was finished with 200 hafnia cycles in the final half period rather than 400.

Crystallinity was measured by x-ray diffraction (XRD) with monochromatic Cu $K\alpha_1$ radiation at diffraction angles below the peaks from the silicon substrate. $K\alpha_1$ photons have a wavelength of 1.5406 A in Cu (Ref. 15), which is used to convert measured diffraction angle θ into crystal lattice spacing d by the Bragg condition, $m\lambda = 2d \sin \theta$. Here λ is the x-ray wavelength and m the integer diffraction order that represents diffraction from successive planes.

Surface roughness was measured on some samples by scanning probe microscopy (SPM) using both the topological and phase-contrast images to get more detailed information about the morphology [16]. Estimates of roughness variation with nanolaminate parameters were obtained from variable angle spectroscopic ellipsometery (VASE) on all samples [17], which also yielded film thickness and refractive index versus wavelength from 280 to 1080 nm. Spectroscopic ellipsometry is a polarization-based technique that measures two quantities, Ψ and Δ, at each wavelength. Ψ is the inverse tangent of the measured intensity ratio of p- and s-polarized components of light reflected from the sample, and Δ is the measured phase difference between those components [18]. These data can be numerically fit to a model to extract the desired parameters, which in this case were film thickness, roughness, and a 3-parameter Cauchy dispersion model described later with the results. Measurement and fitting were done with a VASE instrument and WVASE32 software from J. A. Woollam [19].

The differential 3ω measurements were based on a nominally identical 100 nm ALD alumina reference film applied to all samples. A block diagram of the experiment along with a cross-sectional view of a test sample are shown in Fig. 1. Each sample had a heater and thermometer formed by electron-beam evaporation of 150 nm of aluminum onto the reference alumina, patterned by photolithography and etched to an 8.0 μm wide strip with 1.00 mm length defined by the voltage readout lines in a four-wire resistance measurement configuration. The thickness of the Al line was chosen near the minimum allowable for wire bonding of connections to reduce effects due to its heat capacity [8], and the 8.0 μm width was sufficiently wide relative to the 0.1 μm film thickness to approximate one-dimensional heat flow. The 100 nm films of interest were assembled into test samples in three batches, each batch having its own co-deposited reference sample. Atomic layer deposition alumina was chosen as the reference film due to its excellent electrical insulation properties, extreme uniformity across the deposition area for consistency within each batch [20] and run-to-run repeatability for consistency between batches. The Al temperature coefficient of resistance (TCR) is a very important parameter in this method, and it was measured on every device with two heat/cool cycles from 295–335 K, where its behavior is highly linear. There was some variation in TCR between the three batches but the variation within each batch was smaller than the estimated TCR measurement precision, so the mean TCR was applied to the calculations for each batch as recorded in Table II.

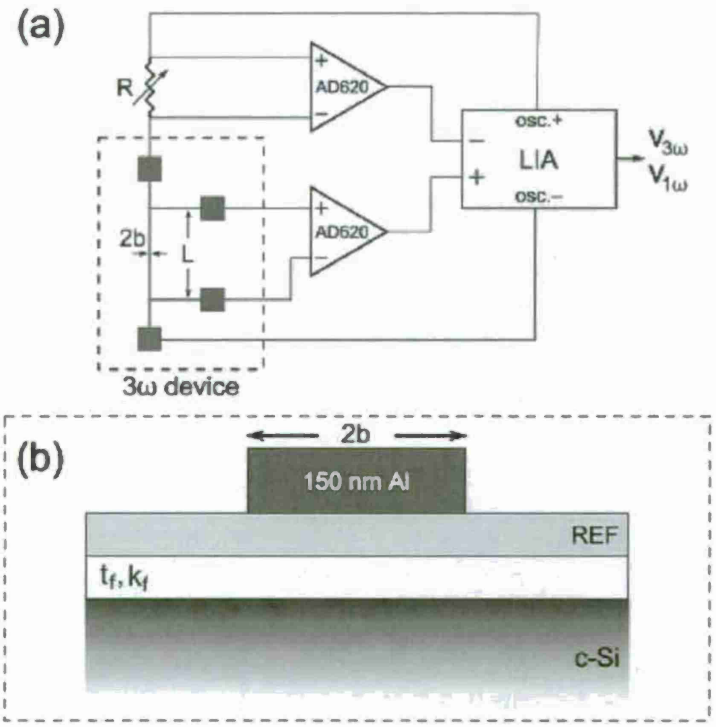

Figure 1 - A diagram of the 3ω experimental setup is shown in panel (a) indicating connections of the device to a series potentiometer, unity-gain AD620 instrumentation amplifiers, and the LIA (lock-in amplifier). In panel (b), a cross-sectional view of a test structure on single-crystal Si indicates the film of interest having thickness t_f and thermal conductivity k_f along with a reference film (REF) and aluminum heater- thermometer; the reference samples for the differential method have the primary film omitted.

A lock-in amplifier (LIA) was used as the sinusoidal input voltage source and as the detection instrument. The very large input heating signal was subtracted from the signal sent to the LIA by a series potentiometer and two identical Analog Devices AD620 instrumentation amplifiers. The readout system is conceptually similar to the one described in detail by Cahill in his original report [10], except that our LIA is digital and can internally select an arbitrary harmonic of the driving signal. The measured 3ω data are shown in Fig. 2. These are converted to experimental DT data using the expression [10,21]

$$\Delta T = \frac{2v_{3\omega}}{\alpha v_{1\omega}}, \qquad (1)$$

where α is the measured TCR of the Al and the v terms are RMS magnitudes of the in-phase third-harmonic and fundamental voltages. As an additional check of the data validity, the slope of the measured ΔT versus ln(ω) can be used to directly estimate the thermal conductivity of the substrate [10], which we found to be consistently near the tabulated 300 K values for silicon [22–24] of 142 to 156 W/(m K). These values are

strongly dependent on temperature in that range and also vary with dopant levels, making this an imprecise verification.

Table 2 – Measured thermal conductivity at room temperature.

Film	k_f (W/m K)	t_f[a] (nm)	Meas. batch[b]
th-SiO_2	1.61	109.6	1
th-SiO_2	1.49	66.5	2
Alumina	2.59	107.7	2
Hafnia	1.72	101.1	2
NL400	1.17	103.1	3
NL200	1.07	110.1	3
NL100	1.02	110.2	2
NL50	1.07	119.7	3
NL20	1.04	105.6	3

[a]Film thickness is excluding the EMA roughness layer included in ellipsometric model for hafnia-containing films.
[b]Batch 1 TCR 0.2864 ± 0.0025 %/K, batch 2 TCR 0.2586 ± 0.0043 %/K, and batch 3 TCR 0.2655 ± 0.0034 %/K.

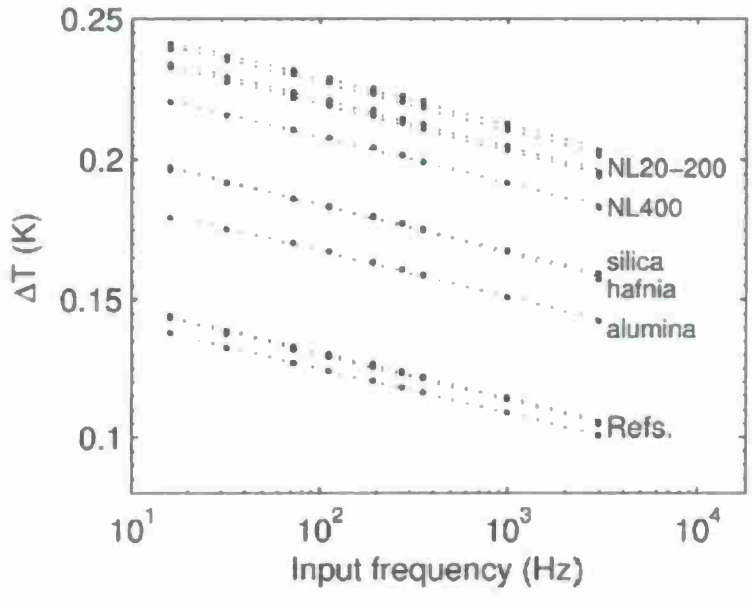

Figure 2 - Measured data from the lock-in amplifier for all of the 100 nm film samples along with the three reference samples, converted to temperature units using Equation 1. The offset relative to the respective reference film is proportional to film thermal conductivity, and the indicated logarithmic linear fits yield estimates of substrate thermal conductivity based on the original 3ω method.

To get a better sense of the role of the hafnia-alumina interfaces in the observed thermal conductivity, cryogenic differential 3ω measurements were performed on the nanolaminate film with highest interface density (NL20) down to the minimum temperature allowed by the TCR of the Al resistor, which was around 30 K. This allows more detailed comparison to interface model predictions. We also measured the pure hafnia film down to 30 K to compare the results to the minimum thermal conductivity model for disordered crystals and amorphous materials [25,26] as has been done for thick sputtered oxides [12]. The TCR in these experiments was measured while slowly heating each sample between the measurement temperatures and comparing the resistance of the device to a calibrated Si diode mounted in the cryostat. The TCR is quite nonlinear over this large range so the derivative of R versus T was used, with some smoothing, to estimate the TCR near each measurement temperature.

A3. Theory

Minimum thermal conductivity model

To describe some of the film results we will apply a minimum thermal conductivity model for amorphous solids developed by Cahill and Pohl [25] and also applied successfully to disordered crystals [26].

$$k_{min} = \left(\frac{\pi}{6}\right)^{1/3} k_B n^{2/3} \sum_m c_m \left(\frac{T}{\Theta_m}\right)^2 \times \int_0^{\Theta_m/T} \frac{x^3 e^x}{\left(e^x - 1\right)^2} dx \qquad (2)$$

T is temperature, n is the atomic number density, c_m is the acoustic velocity of phonon mode m, and Θ_m is the Debye temperature for that mode. The integral can be numerically solved for a given Debye temperature ratio. This model of localized oscillators is applicable when the phonon mean free path is very small, true near room temperature and reasonably accurate down to about 50 K, below which the longer wavelength phonons become more dominant. A primary assumption in the model is that the coupled oscillators have arbitrary phase; this is not true in crystals but does apply to fully disordered materials and is the main reason for its applicability as an effective lower limit to thermal conductivity.

Interface thermal conductivity

We will also discuss the physics of interface behavior as applicable to the nanolaminate films. A note about the definition of interfaces in these films is important before exploring the detailed behavior. The nanolaminate films consist of alternating layers of hafnia of various thickness with fixed ultra-thin layers of alumina. We consider the thickness of these alumina layers to be sufficiently thin such that they serve as a single interface per period, rather than counting one interface at each hafnia-alumina or alumina-hafnia transition for a total of two per period.

Above about 20 K in solids, the diffuse mismatch model (DMM) is a reasonably accurate description of phonon behavior across an interface [27]. The primary

assumption of the DMM is that all phonons are incoherently scattered at the interface; as Swartz and Pohl put it simply in Ref. 27, "each phonon forgets where it came from." Like its lower-temperature cousin the acoustic mismatch model (AMM), the DMM is an elastic scattering model, which means that the energy (frequency) of a scattered phonon does not change during the scattering process. Inelastic processes do occur in real materials and will increase the interface conductance above that predicted by the model, but the effect is not significant in most solid material combinations [27]. This insignificance is because the phonon densities of states in most solids are similar enough that phonons from one material can scatter easily enough into a state at the same energy on the other side of the interface. The exceptions to this rule occur when the interface temperature is well above the Debye temperature of one material but well below that of the other; then inelastic scattering is dominant and the DMM will greatly underestimate the interface conductivity because it would incorrectly predict the reflection of most phonons from the interface.

We apply the usual simplifying assumption that hafnia and alumina behave as Debye solids in this temperature range, with the phonon density of states per unit volume $D_m(\omega)$ of each mode m (one longitudinal and two transverse) described by [28] a sound velocity c_m:

$$D_m(\omega) = \frac{\omega^2}{2\pi^2 c_m^3}. \tag{3}$$

The number of phonons in each mode at a given frequency at a specific temperature, Nm(x, T), is the product of the density of states and the Bose-Einstein occupancy factor, yielding

$$N_m(\omega, T) = \frac{D_m(\omega)}{\exp\left(\frac{\hbar\omega}{k_B T}\right) - 1}, \tag{4}$$

where k_B is the Boltzmann constant.

Under this Debye simplification, both the AMM and DMM are described by the same equation for thermal boundary conductivity based on the acoustic velocities c_m, integrated transmission probabilities Γ_m, and phonon number densities N_m for each of the three acoustic phonon modes m:

$$h_{\mathrm{Bd}} = \frac{1}{2}\sum_m c_{1,m}\Gamma_{1,m}\int_0^{\omega_1^D} \hbar\omega \frac{dN_{1,m}(\omega, T)}{dT} d\omega \tag{5}$$

The only parameter that differs between the two models is Γ, the integrated transmission probability, which is where the specular versus diffuse scattering assumptions manifest. In the DMM, Γ does not depend on incident angle; it is a ratio of acoustic velocities on each side of the interface for each of three acoustic modes:

$$\Gamma_1^{DMM} = \frac{1}{2}\frac{\sum_m c_{2,m}^{-2}}{\sum_m c_{1,m}^{-2} + \sum_m c_{2,m}^{-2}}. \quad (6)$$

Applying Eq. (6) and the temperature derivative of Eq. (4) to Eq. (5) yields the following DMM boundary conductivity expression that we compared to our measured data:

$$h_{Bd} = \frac{1}{8\pi^2 k_B T^2}\frac{\left(\sum_m c_{1,m}^{-2}\right)\left(\sum_m c_{2,m}^{-2}\right)}{\sum_m c_{1,m}^{-2} + \sum_m c_{2,m}^{-2}} \times \int_0^{\omega_1^D} \frac{\hbar^2\omega^4 d\omega \exp\left(\frac{\hbar\omega}{k_B T}\right)}{\left[\exp\left(\frac{\hbar\omega}{k_B T}\right) - 1\right]^2} \quad (7)$$

The model inputs are thus temperature T, acoustic velocities for the longitudinal and two transverse modes for both materials $c_{i,L}$ and $c_{i,t}$, and the lowest of the two materials' Debye cutoff frequency, ω_1^D. In the low-temperature limit, Eq. (7) has a simpler, T^3, dependence just like Debye heat capacity, but in this case the full expression was numerically integrated to cover the entire temperature range of interest. The ħ constants were left in the integral to balance the ω terms since ω_D is roughly 10^{13} rad/s. Note the similarity of this integral to that in Eq. (2) since both are based on Debye models.

Differential 3ω model

The model for extracting film thermal conductivity from the differential 3x method is [8]

$$k_f = \frac{t_f}{2bL}\frac{1}{(\Delta T/P)_f - (\Delta T/P)_{REF}} \quad (8)$$

The subscripts *f* and REF represent the film and reference samples, the measured temperature differences ΔT are given by Eq. (1), b and L are the half width and length of the metal lines, t_f is the film thickness, and P is the average input power calculated from $V^2_{1\omega}/R$ where R is device electrical resistance at P measured using the balanced potentiometer. Many of the parameters are also indicated in Fig. 1. Equation (8) is derived from a simple one-dimensional heat flow model where the reference film(s) and

the film of interest both contribute a thermal conductance of $G_i = 2bLk_i/t_i$, and these G_i terms are added inversely. It is important to note that the contribution of the reference film(s) only cancel out to yield Eq. (8) if both samples have the same width 2b and length L and see the same input power P. This matching of area and power input per unit length causes a $(2bLk/t)_{REF}$ reference-film term to cancel, as well as a more complicated thermal diffusivity term from the 3ω substrate model [10].

A4. Results and Discussion

Crystallinity

The x-ray diffraction results are presented in Fig. 3. A broad amorphous peak with maximum at $2\theta = 32°$ is found in all nanolaminates, but they have none of the many crystalline monoclinic hafnia peaks that are evident in the pure hafnia film. This is a significant result, since previous work on similar nanolaminate films suggested that x-ray-observable crystallinity appeared with hafnia layers greater than 10 nm (100 ALD cycles) (Ref. 4). We see no such crystallinity through 20 nm or 200 ALD cycles per period, potentially significant for applications where alumina content should be minimized. There may be very minor crystalline peaks in NL400, appearing as small bumps at some of the monoclinic peak locations. This is not entirely unprecedented according to previous TDMAH-based ALD hafnia reports: a film 33nm thick (330 ALD cycles) was found to be amorphous by XRD while a nominally identical film at twice that thickness was partially crystalline [5], and similar ALD hafnia films 20–30 nm thick were also x-ray amorphous [14].

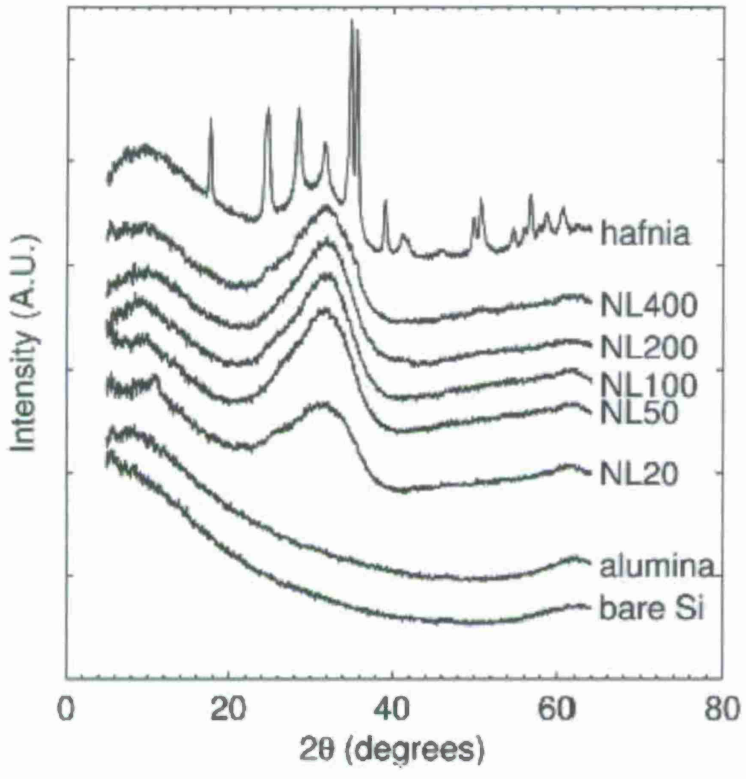

Figure 3 - X-ray diffraction results showing the amorphous or nearly amorphous nature of alumina and all of the nanolaminate films, which are labeled as defined in Table I with the number of hafnia ALD cycles per period. The hafnia film has over twenty monoclinic crystalline peaks and is about 14–32% crystalline based on the relative area under amorphous and crystalline regions.

The percentage of crystallinity of the pure hafnia film can be determined by the area under all of the crystalline peaks relative to the area under the much broader amorphous "peaks." This determination is sensitive to the choice of background or baseline shape. Choosing a baseline shape that matches the shape of the measured bare Si data yields a hafnia crystallinity of about 14%. An alternative is to choose a linear background that follows the general slope of the measured pattern without resulting in a negative number of counts for any value of 2θ. This background yielded a crystallinity of 32%, which is larger because it cutoff some regions previously included in the amorphous area. The actual percent crystallinity likely falls somewhere between these two values.

Also noteworthy is a peak near $2\theta = 11^\circ$ in NL20 that corresponds to a lattice spacing of about 0.8 nm using the Bragg condition and x-ray wavelength. That measured spacing is similar to the nanolaminate period of the film, since it has 40 periods of hafnia-alumina pairs formed from 20 ALD cycles of hafnia and 5 ALD cycles of alumina. Based on the 0.1 nm/cycle growth, each period is expected to be about 2.0 nm of hafnia and 0.5 nm of alumina. Wide-angle XRD is not a particularly sensitive way to measure the spacing of such a film structure but it is indicative of order in the film near the expected scale. The other films have at least twice the interface spacing (and at most half the number of interfaces) as NL20, so any diffraction from them would likely occur at 2θ less than or about equal to 5° (and lower in intensity by at least half).

Surface roughness and refractive index

The scanning probe microscopy data for the hafnia in Fig. 4 and the NL100 film in Fig. 5 show that the expected large drop in surface roughness with incorporation of alumina does indeed occur, from 6.3 nm root mean square (RMS) to 0.75 nm RMS, corroborating the results of Hausmann and Gordon [4]. The alumina film and the bare substrate were also measured and all four results are summarized in Fig. 6.

We are particularly interested in the optical behavior of these films, considering the demonstrated high laser-induced damage threshold of hafnia,29 in-part due to its relatively high bandgap energy [30]. With alumina interlayers on the order of only 0.5 nm, much shorter than visible wavelengths, we expect each nanolaminate to behave as an effective refractive index based on relative alumina content. The spectroscopic ellipsometry data were fit to a Cauchy model for each film with thickness along with three free parameters representing dispersion.

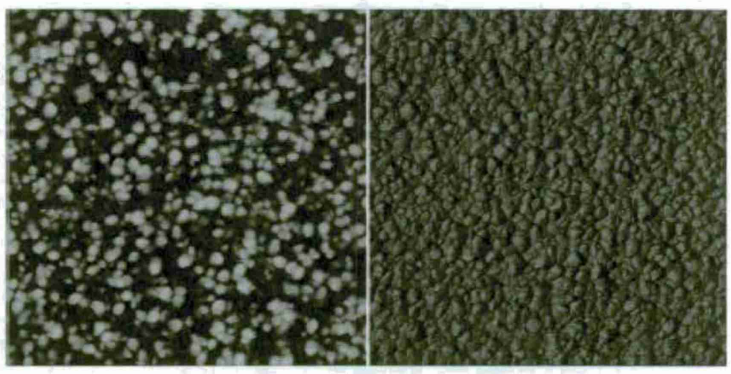

Figure 4 - Scanning probe microscopy results on a ~100 nm thick hafnia film, indicating a large surface roughness of 6.3 nm RMS. The topographic image on the left has a pixel range of 0–30 nm and covers a 2 μm by 2 μm area. The phase-contrast image on the right covers the same lateral area, giving a clearer look at the boundaries between surface features.

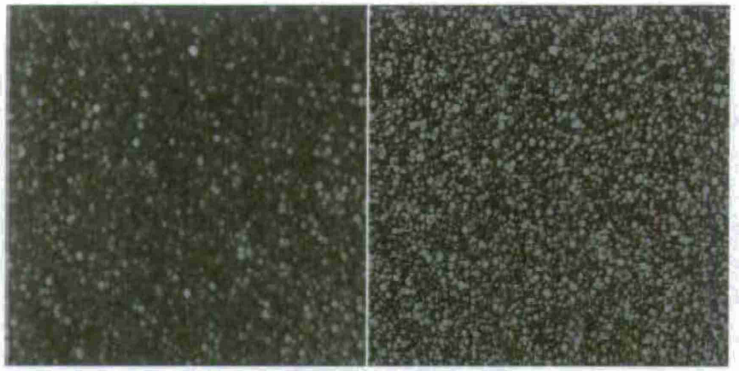

Figure 5 - SPM results on NL100, a 100 nm thick hafnia nanolaminate film having 100 layers (~10 nm) of hafnia per period. The topographic (left) and phase-contrast (right) images correspond to those in Fig. 4 except the pixel range is reduced by half (to 0–15 nm) in this case. This nanolaminate film is quite smooth, 0.75 nm RMS, and lacks the well-defined regions on the surface.

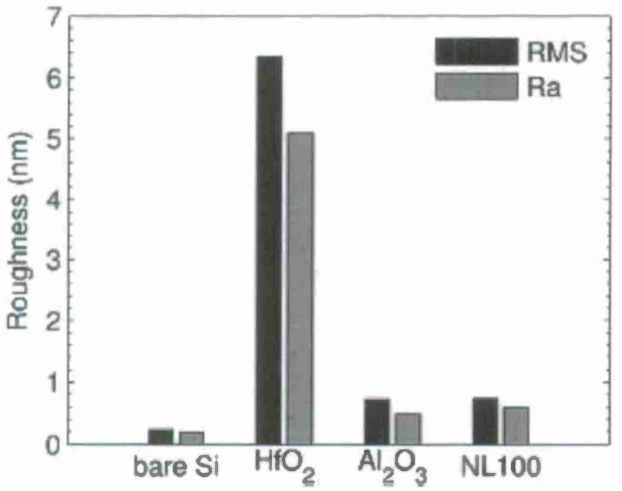

Figure 6 - A summary of SPM surface roughness results, with RMS and arithmetic average (Ra) roughness measures shown for the bare Si, hafnia from Fig. 4, alumina, and NL100 from Fig. 5. This nanolaminate film is as smooth as the alumina, and much more suitable for optical applications than the partially crystalline crystalline hafnia.

$$n(\lambda) = A + \frac{B}{\lambda^2} + \frac{C}{\lambda^4} \qquad (9)$$

This three-parameter model fit the ellipsometric data very well for the nanolaminate films, with refractive index versus wavelength maintaining a shape like the hafnia film. The expected reduction in refractive index with increasing alumina composition was observed, as shown in Fig. 7 for some selected wavelengths.

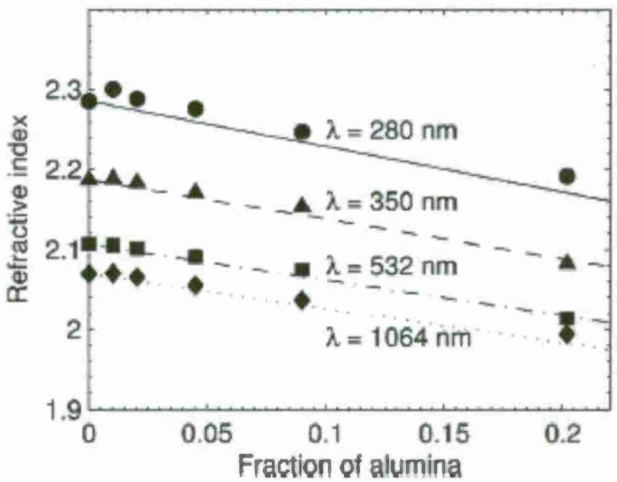

Figure 7 - Hafnia and nanolaminate refractive index versus composition for selected wavelengths along with a model for each based on a linear combination of measured hafnia and alumina refractive indices. Wavelengths shown are 280 nm (circles), 350 nm (triangles), 532 nm (squares), and 1064 nm (diamonds).

Since each ellipsometric dataset contained 81 wavelength steps from 280 nm to 1080 nm, each wavelength having both a W and a D datapoint representing reflected polarization amplitude and phase ratios, the solution to each system was highly over-constrained, allowing an additional layer to be included in the fit to represent surface roughness. This effective- medium approximation (EMA) layer was set to match the fitted film dispersion according to Eq. (9) but also consist of 50% voids having a refractive index of one. The thickness of the EMA layer was allowed to vary along with the other four parameters, and a reasonable solution was obtained in each case with little correlation between model parameters except in the most extreme nanolaminate (NL20). A solution to the model was reached for NL20 as well, but there was a large amount of correlation between the parameters, especially thickness and EMA roughness. As in any model fitting, the correlation means that those data were not sufficient to determine roughness. None of the other films showed this correlation behavior. The shorter-wavelength portion of the model was particularly sensitive to the EMA roughness parameter for surface roughness of this magnitude and was especially helpful in the fitting. Roughness is plotted as a function of alumina concentration in Fig. 8, showing good agreement with the subset of SPM results from Fig. 6. We see that even the most

moderate nanolaminate, NL400, has fairly low roughness relative to the pure hafnia film. This is expected considering that we found nearly all of our nanolaminate films to be x-ray amorphous, but it was surprising considering the previously reported maximum of roughly 100 hafnia layers per period for smooth, amorphous films [4]. That work did suggest a strong temperature dependence of crystallinity in the vicinity of 250°C, so it is plausible that moderate temperature variations or measurement uncertainty at various points in the deposition chamber could significantly affect these film properties.

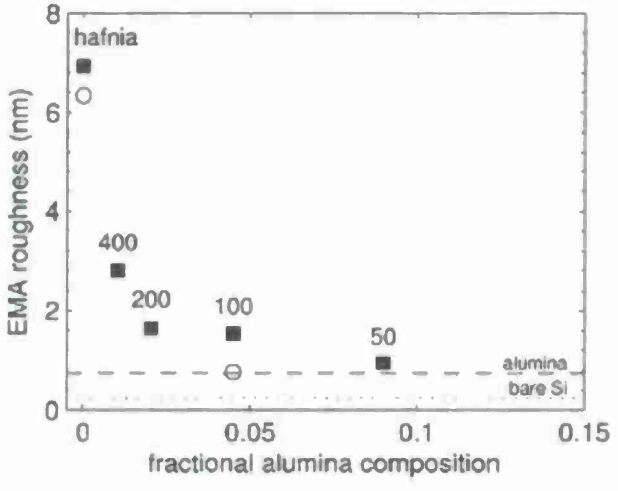

Figure 8 - Roughness values of all films obtained from VASE measurements as a function of alumina composition. Roughness here is the thickness of a 50% void effective-medium approximation (EMA) layer included in the fits to ellipsometric data. Open circles and dashed and dotted lines show RMS values values from SPM data in Fig. 6 for comparison.

Room-temperature thermal conductivity

Thermally grown silica films were included to verify the accuracy of this implementation of the differential 3ω thermal conductivity measurement technique. A 109.5 nm thick SiO_2 film had a measured thermal conductivity of 1.61W/(m K) at room temperature, and a 66.5 nm film was measured to be 1.49 W/(m K). These are slightly above but reasonably close to reported values [12]. All room-temperature results are shown in Table II, along with important parameters. The alumina film has a relatively high thermal conductivity, and the partially crystalline hafnia film has a thermal conductivity about 50–60% larger than that of the nanolaminates.

The variation of thermal conductivity among the nanolaminates contains important information about the behavior of the constituent films. We can immediately see from Table II that the nanolaminates all have very similar thermal conductivity. These are plotted versus interface density in Fig. 9 along with several models. The first case is that the hafnia and alumina layers behave as a series combination of individual layer thermal resistance, with zero interfacial resistance. The dependence is then on alumina concentration rather than interface density, not matching the observed behavior. Another

possibility is that each hafnia layer is in series with the interface resistance, with two free parameters of intrinsic (amorphous) hafnia thermal conductivity and interface conductivity that are fit to the data using least squares, resulting in 1.10 W/(m K) and 1.5 GW/(m^2 K). The former value is quite reasonable based on these data and previously reported hafnia film results [3,12], but the latter is about two times higher than what is expected for any solid-solid interfaces [31]. This indicates that the interface conductivity is on the same order as the individual layer thermal conductivity, at the low end of the detectable range using this technique. A final model variant is also plotted in Fig. 9, using the minimum thermal conductivity model result of 1.04 W/(m K) from Eq. (2) for the hafnia layers and the DMM result of 500 MW/(m^2 K) from Eq. (7) calculated for these interfaces. We used estimated acoustic velocities for alumina and hafnia [32] and Debye temperatures based on atomic number density calculated from reported mass densities for a fully-dense amorphous alumina film [12] of 3.51 g/cm^3 and for ALD hafnia [13] of 9.23 g/cm^3.

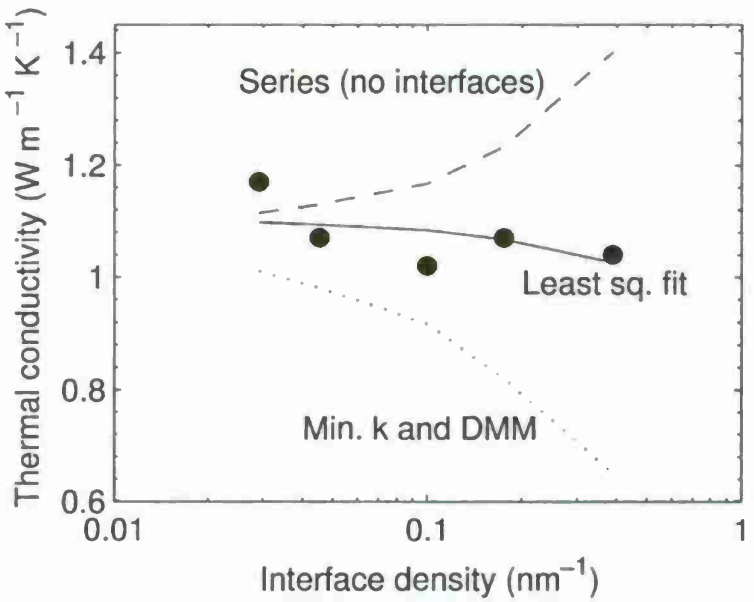

Figure 9 - The measured thermal conductivity of the nanolaminate films are shown versus interface density along with several models. The dashed line is a model with no interface resistance, the solid line is a least squares fit to hafnia intrinsic thermal conductivity (1.10 W/m K) and interface conductance (1.5 GW/m^{2}K), and the dotted line is the same model but with parameters calculated from the minimum thermal conductivity model [Eq. (2)] and DMM [(Eq. (7)].

Cryogenic thermal conductivity

The measured 30–300 K data for the pure hafnia film along with NL20, the nanolaminate film with hafnia layers approximately 2 nm thick, are shown in Fig. 10 along with minimum thermal conductivity and diffuse mismatch models calculated from Eqs. (2) and (7) using the aforementioned parameters.

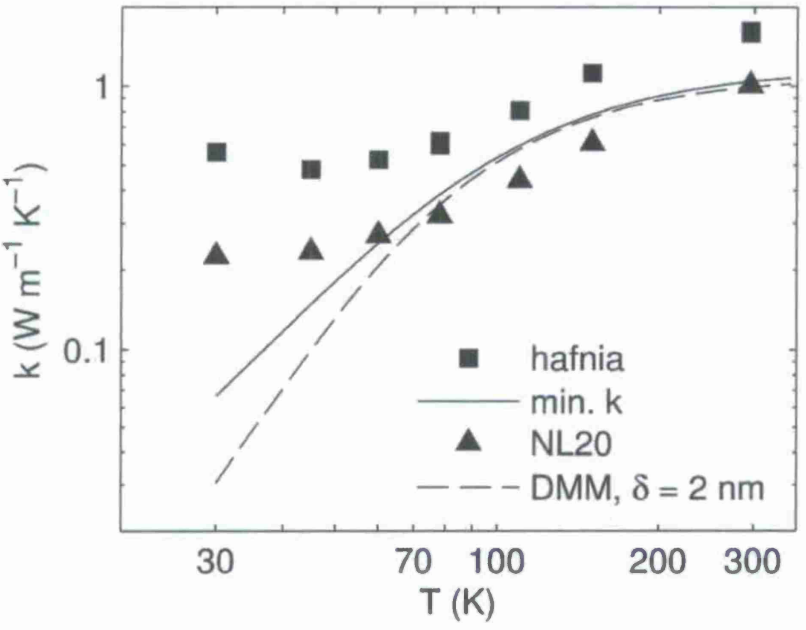

Figure 10 - The measured thermal conductivity of the hafnia film (squares) and NL20 (triangles) are shown with two models based on Debye parameters of acoustic velocities and atomic number density; a minimum thermal conductivity model for hafnia (solid line), and a diffuse mismatch model for alumina-hafnia interfaces assuming interface-dominated conductivity with 2nm interface spacing (dashed line).

The hafnia film has a significantly higher thermal conductivity than predicted by the minimum thermal conductivity model but a similar temperature dependence. This is comparable to a previous result for sputtered hafnia [12]. Here, we measured to a lower temperature, and the observed slight increase in thermal conductivity near 30 K in Fig. 10 may be indicative of crystalline-like behavior beginning to dominate, or it may simply be due to the greater uncertainty as the TCR of the Al resistor approaches zero, becoming more difficult to measure accurately and also reducing the 3ω signal.

We see in Fig. 10 that at temperatures above about 80 K, the NL20 film could be described equally well by a minimum thermal conductivity model or an interface-dominated diffuse mismatch model. This result could be interpreted in several different ways. The very thin alumina interlayers may simply be serving their intended role of disrupting all hafnia crystallite growth, yielding phonon behavior like a fully amorphous hafnia as described by the minimum thermal conductivity model. Alternatively, the hafnia-alumina interfaces could be completely dominating the thermal conductivity and yielding behavior predicted by the DMM with 2 nm interface spacing, or the interfaces and amorphous hafnia film regions could be contributing equally. These three possibilities cannot be easily separated.

The divergence of the NL20 data from both models below about 80 K in Fig. 10 is expected because the dominant phonon wavelength in real materials is inversely proportional to temperature, but neither model fully captures the effect. The minimum

thermal conductivity model (solid line) is based on local oscillators, but as the dominant phonon wavelength increases with decreasing temperature the localized model becomes less accurate, predicting an excessive decrease in thermal conductivity. In the case of interface resistance based on the DMM (dashed line), the interface model itself is quite accurate through this range [27], but the assumption of interface-dominated thermal resistance in this nanolaminate breaks down, also due to the longer wavelength phonons, so that the effective thermal conductivity can no longer reasonably be described as $k \sim \delta G_{DMM}$ where δ is interface spacing and G_{DMM} the interface conductivity.

It is interesting to compare the temperature behavior of this nanolaminate to that observed in semiconductor superlattices, which have periodic layers at a similar order of magnitude but where the layers are crystalline and have complicated electron and phonon band structures. GaAs-AlAs superlattices have yielded increasing thermal conductivity with decreasing temperature [33]. That behavior is the opposite of what we see in NL20 but is generally expected for high-quality crystals, mostly due to the increased phonon mean free path in the crystalline layers with decreasing temperature. In contrast, Si-Ge superlattices have shown behavior more like that seen here in NL20, with thermal conductivity decreasing with temperature [34]. In the longer-period Si-Ge structures this was attributed to the relatively poor crystal quality due to defects induced by lattice mismatch, and in shorter-period structures the interfaces were suspected to be playing a large role due to the very different phonon band structure in Si and Ge.

Measurements below 30 K would be useful to observe the transition from diffuse to specular scattering expected near 20 K in most solids and described by the acoustic mismatch model [27], but below 30 K the temperature-dependence of the aluminum resistor quickly becomes too close to zero, diminishing the 3ω signal below the measurement threshold. Similar issues have been observed in 3ω measurements using silver resistors [26] and are a difficult limitation of the 3ω methods.

B.) Absorption and Laser Damage Testing of ALD coatings

During the program, we sent substrates coated with ALD Al_2O_3 and substrates coated with HfO_2 to be tested for refractive index crystal structure, optical absorption, and pulsed laser damage threshold. This work was a collaboration with other JTO-funded groups at Colorado State University (in collaboration with Prof. Carmen Menoni), Stanford University (in collaboration with Dr. Ashot Markosyan), and the University of New Mexico (in collaboration with Prof. Wolfgang Rudolph). As part of this collaboration, we also measured (at the University of Minnesota) the thermal conductivity of Sc_2O_3 films from Colorado State University. Much of the data was collected into a powerpoint summary by CSU and sent to our group, and we reproduce a representative subset of the data in this report.

The most important sections are B4 and B5 where the absorption and the pulsed laser damage threshold are reported. Both show high performance, but the absorption is of particular note because it shows that these ALD films have performance comparable to the best commercial ion-beam sputtered (IBS) films, which are the "gold standard" for low absorption films.

B1. Substrates

The CVI-Melles-Griot fused silica substrates were provided by CSU. We deposited four samples deposited with ALD films at 250°C. There was also a bare reference sample.

1) 100nm of Al_2O_3
2) bilayer of 100nm Al_2O_3/ 100nm HfO_2
3) 100nm of HfO_2
4) 100nm of HfO_2
5) bare reference sample

B2. Refractive Index

This data on refractive index was performed using an ellipsometer at CSU and supports previous similar data taken at Minnesota, for example, as seen in Figure 7 above. The refractive index of ALD Al_2O_3 at λ = 1μm was 1.64, and the refractive index of ALD HfO_2 at λ = 1μm was 2.06.

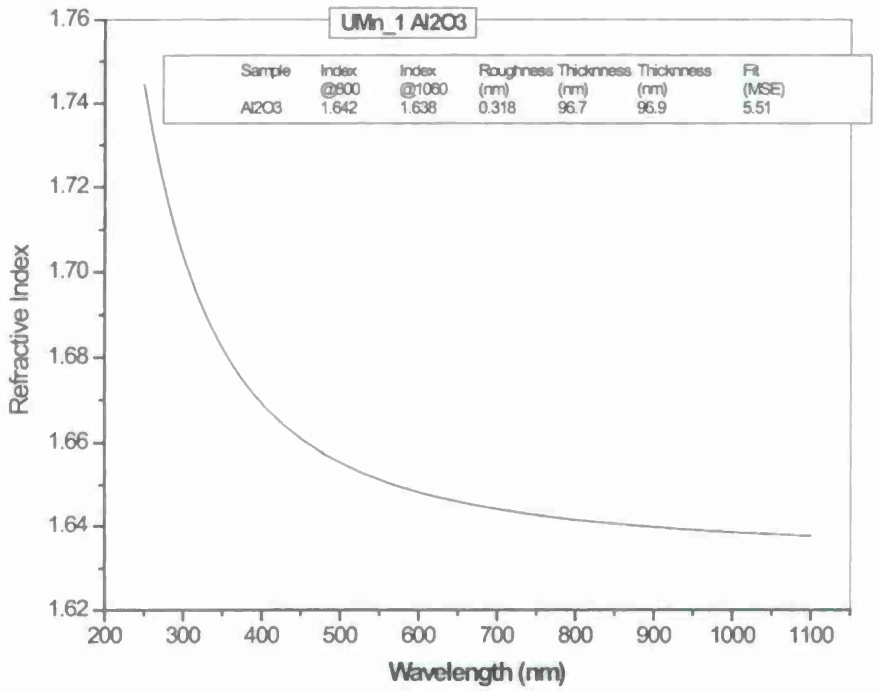

Figure 11 – Refractive index versus wavelength of an ALD Al_2O_3 film.

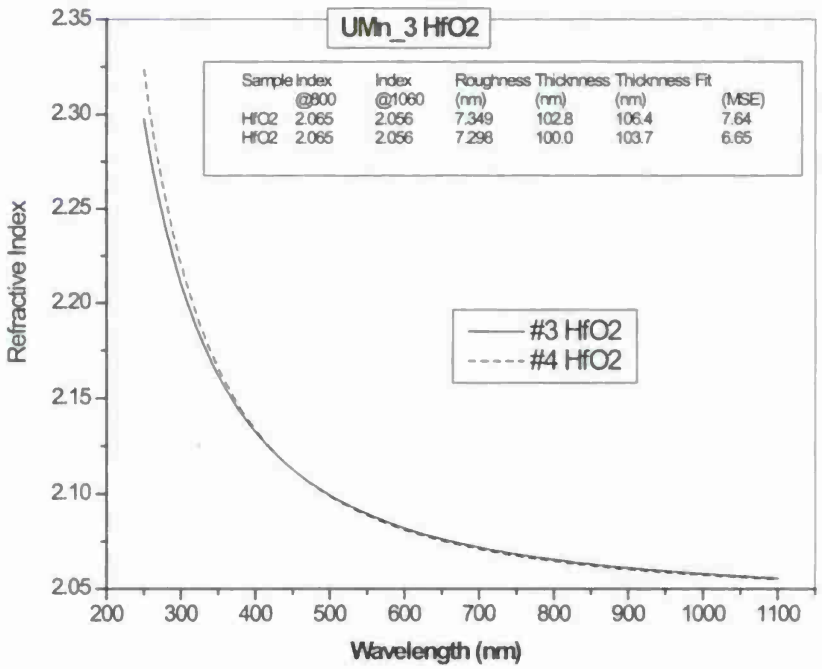

Figure 12 - Refractive index versus wavelength of two ALD HfO_2 films.

B3. Crystal structure using X-ray Diffraction

The data taken at Minnesota presented in the previous section for ALD films (see Figure 3) clearly shows that alumina deposited at 250°C is amorphous while hafnia is partially polycrystalline. Carmen Menoni and her group at CSU also performed XRD measurements of ALD HfO_2 and achieved similar results.

From CSU's slides: The nanocrystallinity of HfO_2 was investigated at CSU using glancing angle x-ray diffraction (GAXRD) measurements, which were made at a fixed shallow incidence angle of 0.5°. Detector scans were done to measure the diffracted intensity of Cu Kα x-rays as a function of 2Θ using a Bruker D-8 Discover instrument.

These results show clear evidence of nano-crystallinity in the ALD HfO_2. The two University (CSU and UM) XRD spectra do seem to agree with the positions of the peaks; however, the absence of the broad peak and the distinct intensity of the nano-crystallites may stems from the penetration depths between the measurements. This spectra shows the absence of broad features from the substrate, which were seen in UM measurements and may therefore lead to better resolved crystalline peaks.

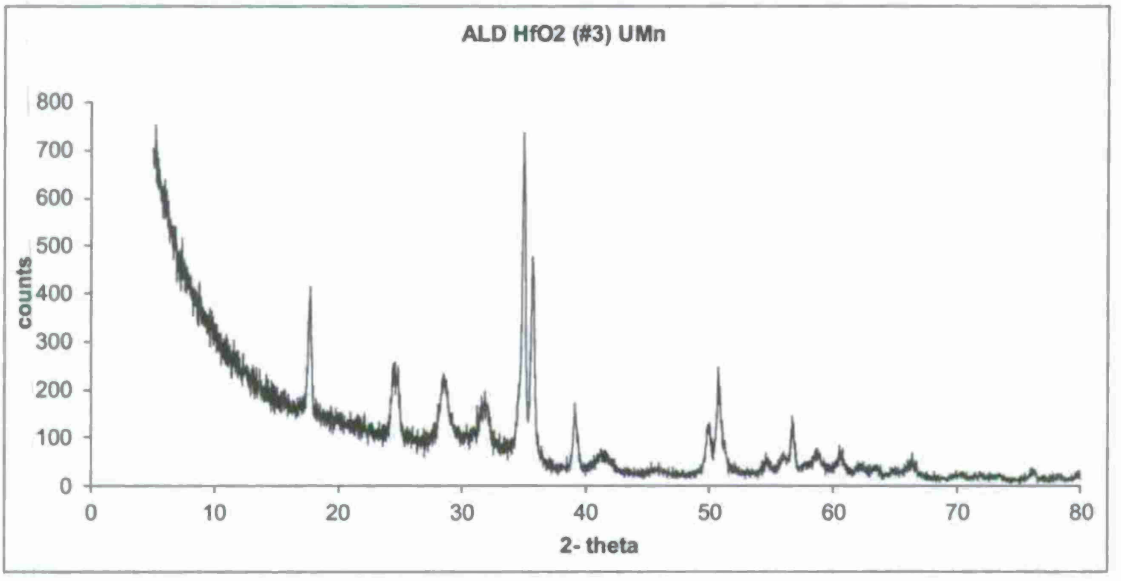

Figure 13 – XRD measurement from CSU of sample 3, which was a 100nm ALD HfO_2 film on fused silica. The data shows clear polycrystallinity. The Al_2O_3 films were amorphous.

B4. Absorption

The absorption of the films was tested by Dr. Ashot Markosyan of Stanford University using a photothermal common path interferometry (PCI) system. The resulting data is shown in the table and figures below. Average absorptions vary from 0.9ppm to 1.05ppm, which are state-of-the-art numbers for optical coatings.

Single layers of ALD	PCI Loss (ppm)
Al2O3 (#1)	0.9
Al2O3/HfO2 bi-layer (#2)	1.03
HfO2 (#3)	1.05
HfO2 (#4)	0.93

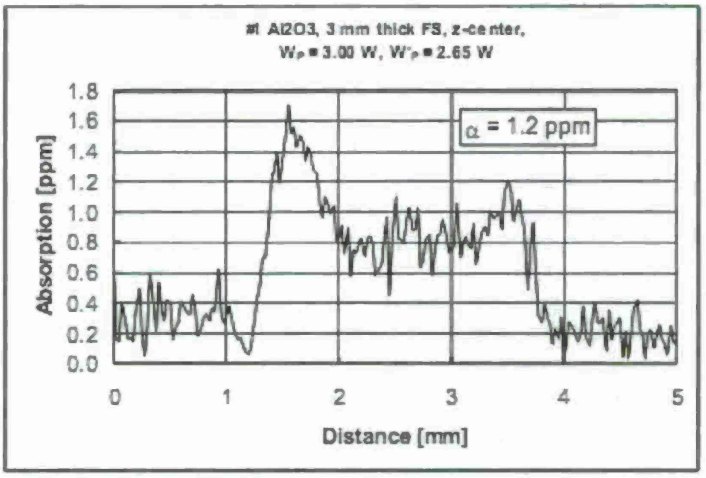

Figure 14 – Photothermal common-path interferometry (PCI) measurement of the absorption of an alumina-coated fused silica substrate as a function of distance across the surface of the wafer.

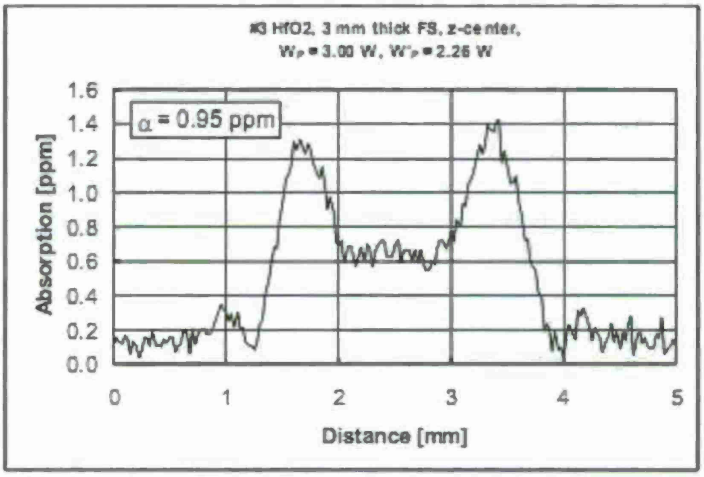

Figure 15 - Photothermal common-path interferometry (PCI) measurement of the absorption of a hafnia-coated fused silica substrate as a function of distance across the surface of the wafer.

B5. Pulsed Laser Damage Threshold

The pulsed laser damage threshold of the films was tested by the research group of Wolfgang Rudolph at the University of New Mexico. It should be noted that the most relevant laser damage threshold for typical directed energy applications is a continuous wave laser thermal breakdown, but since this type of breakdown is poorly documented in the literature, a pulsed laser damage threshold is the only common metric that is available for specifying damage resistance.

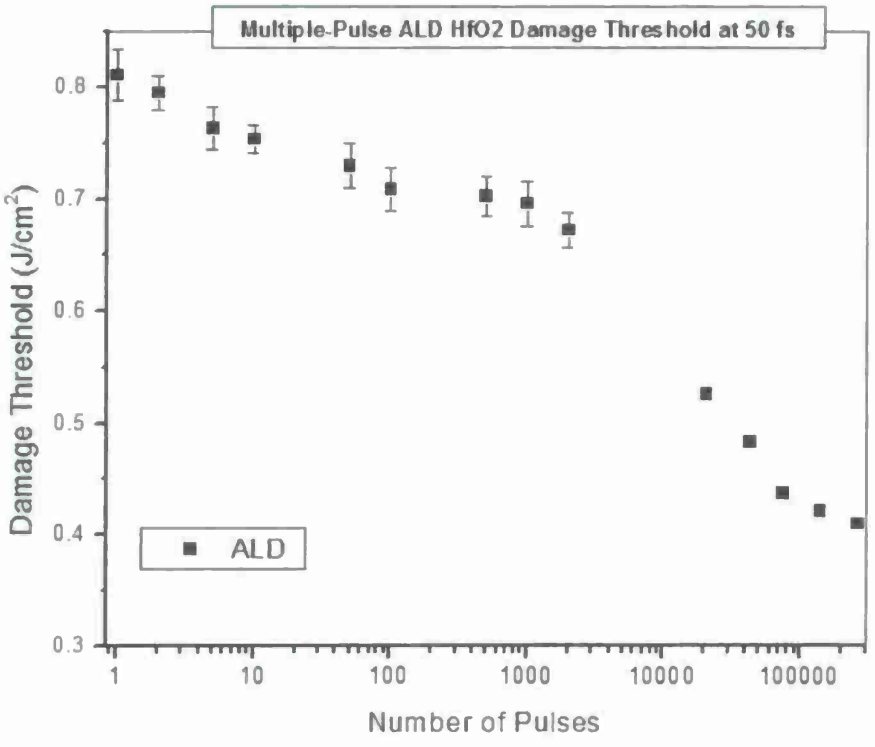

Figure 16 – Damage threshold vs. number of pulses for an ALD HfO_2-coated fused silica substrate.

From the CSU Slides: The results of the multipulse damage shows reduced damage threshold going from a single pulse towards an infinite number of pulses, F_∞, for the HfO_2 ALD. This variation of damage with number of pulses is typical of other oxides. The explanation of the decrease in the damage with increasing number of excitation pulses is that there is an accumulation of laser-induced defects at fluence values below single-shot breakdown. At F_∞ the number of laser-induced defects saturates.

B6. Thermal Conductivity of Scandium Oxide

The research group at CSU was performing a JTO-related investigation of scandium oxide, Sc_2O_3, which was thought to have potentially useful properties for high-power laser coatings. However, they did not have the capability to measure the thermal conductivity of their films, so we collaborated to measure this property using our cryogenic system described in Part A.

The measured thermal conductivity values as a function of temperature are shown in Figure 17. They show behavior that is typical of optical coating oxides in both magnitude and functional form.

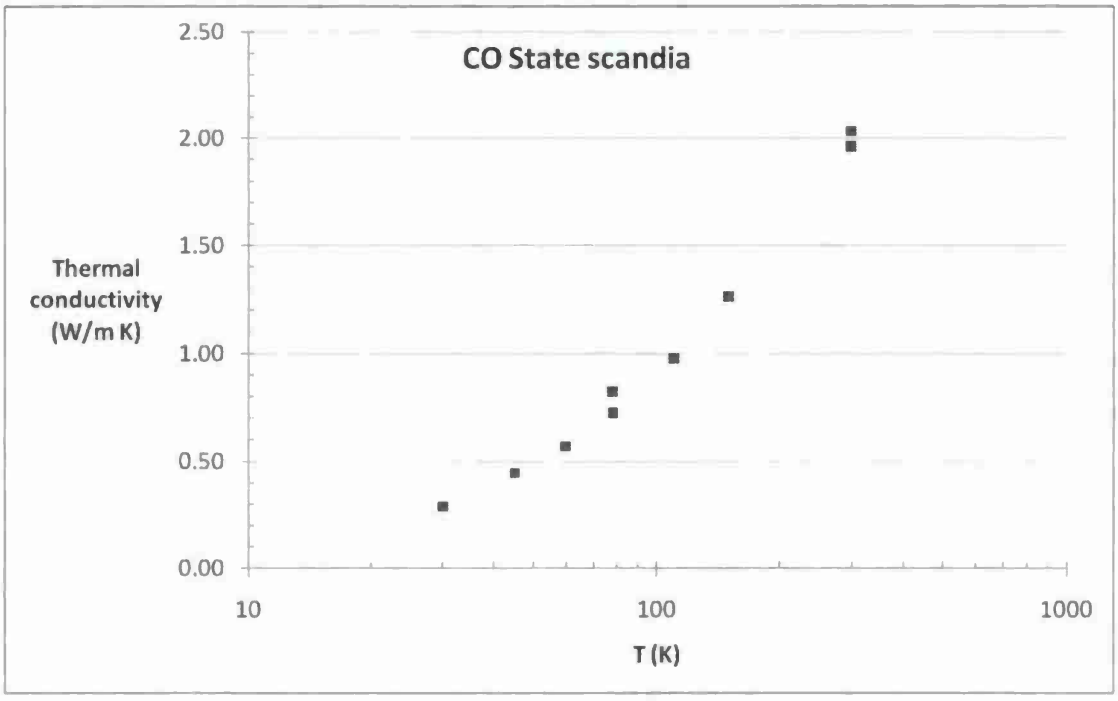

Figure 17 – Thermal conductivity versus temperature of a scandium oxide film measure using a cryogenic differential 3ω method.

IV. References:

[1] K. Mistry, C. Allen, C. Auth, B. Beattie, D. Bergstrom, M. Bost, M. Brazier, M. Buehler, A. Cappellani, R. Chau, C. Choi, G. Ding, K. Fischer, T. Ghani, R. Grover, W. Han, D. Hanken, M. Hattendorf, J. He, J. Hicks, R. Huessner, D. Ingerly, P. Jain, R. James, L. Jong, S. Joshi, C. Kenyon, K. Kuhn, K. Lee, H. Liu, J. Maiz, B. McIntyre, P. Moon, J. Neirynck, S. Pae, C. Parker, D. Parsons, C. Prasad, L. Pipes, M. Prince, P. Ranade, T. Reynolds, J. Sandford, L. Shifren, J. Sebastian, J. Seiple, D. Simon, S. Sivakumar, P. Smith, C. Thomas, T. Troeger, P. Vandervoorn, S. Williams, and K. Zawadzki, in *Technical Digest of IEEE International Electron Device Meeting* (IEDM) (IEEE, Washington, DC, 2007) pp. 247–250.

[2] "Front End Processes" International Technology Roadmap for Semiconductors (ITRS, http://www.itrs.net/Links/2009ITRS/Home2009.htm, 2009).

[3] M. Panzer, M. Shandalov, J. Rowlette, Y. Oshima, Y. W. Chen, P. McIntyre, and K. Goodson, *Electron Device Lett.* 30, 1269 (2009).

[4] D. M. Hausmann and R. G. Gordon, *J. Cryst. Growth* 249, 251 (2003).

[5] J. C. Hackley and T. Gougousi, *Thin Solid Films* 517, 6576 (2009).

[6] S.-I. Zaitsu, S. Motokoshi, T. Jitsuno, M. Nakatsuka, and T. Yamanaka, *Jpn. J. Appl. Phys.* 43, 1034 (2004).

[7] R. M. Costescu, D. G. Cahill, F. H. Fabreguette, Z. A. Sechrist, and S. M. George, *Science* 303, 989 (2004).

[8] T. Borca-Tasciuc, A. R. Kumar, and G. Chen, *Rev. Sci. Instrum.* 72, 2139 (2001).

[9] G. Pernot, M. Stoffel, I. Savic, F. Pezzoli, P. Chen, G. Savelli, A. Jacquot, J. Schumann, U. Denker, I. Mo¨nch, C. Deneke, O. G. Schmidt, J. M. Rampnoux, S. Wang, M. Plissonnier, A. Rastelli, S. Dilhaire, and N. Mingo, *Nat. Mater.* 9, 491 (2010).

[10] D. G. Cahill, *Rev. Sci. Instrum.* 61, 802 (1990).

[11] D. G. Cahill, M. Katiyar, and J. R. Abelson, *Phys. Rev. B* 50, 6077 (1994).

[12] S. Lee, D. G. Cahill, and T. H. Allen, *Phys. Rev. B* 52, 253 (1995).

[13] D. M. Hausmann, E. Kim, J. Becker, and R. G. Gordon, Chem. Mater. 14, 4350 (2002).

[14] K. Kukli, T. Pilvi, M. Ritala, T. Sajavaara, J. Lu, and M. Leskela¨, Thin Solid Films 491, 328 (2005).

[15] J. Rousseau, Basic Crystallography (Wiley, New York, England, 1998) p.128.

[16] G. K. H. Pang, K. Z. Baba-Kishi, and A. Patel, Ultramicroscopy 81, 35 (2000).

[17] D. E. Aspnes, J. B. Theeten, and F. Hottier, Phys. Rev. B 20, 3292 (1979).

[18] G. Jellison, Jr., Thin Solid Films 234, 416 (1993).

[19] J. A. Woollam, B. D. Johs, C. M. Herzinger, J. N. Hilfiker, R. A. Synowicki, and C. L. Bungay, in Proceedings of SPIE, CR72, 3 (1999).

[20] N. T. Gabriel and J. J. Talghader, Appl. Opt. 49, 1242 (2010).

[21] D. G. Cahill, Rev. Sci. Instrum. 73, 3701 (2002).

[22] H. R. Shanks, P. D. Maycock, P. H. Sidles, and G. C. Danielson, Phys. Review 130, 1743 (1963).

[23] C. J. Glassbrenner and G. A. Slack, Phys. Rev. 134, A1058 (1964).

[24] P. Maycock, Solid-State Electron. 10, 161 (1967).

[25] D. G. Cahill and R. O. Pohl, Solid State Commun. 70, 927 (1989).

[26] D. G. Cahill, S. K. Watson, and R. O. Pohl, Phys. Rev. B 46, 6131 (1992).

[27] E. T. Swartz and R. O. Pohl, Rev. Mod. Phys. 61, 605 (1989).

[28] For example, see C. Kittel and P. McEuen, Introduction to Solid State Physics, 8th ed. (Wiley, New York, 2005), p.112.

[29] M. Alvisi, M. Di Giulio, S. G. Marrone, M. R. Perrone, M. L. Protopapa, A. Valentini, and L. Vasanelli, Thin Solid Films 358, 250 (2000).

[30] M. Mero, J. Liu, W. Rudolph, D. Ristau, and K. Starke, Phys. Rev. B 71, 115109 (2005).

[31] D. G. Cahill, W. K. Ford, K. E. Goodson, G. D. Mahan, A. Majumdar, H. J. Maris, R. Merlin, and S. R. Phillpot, J. Appl. Phys. 93, 793 (2003).

[32] We applied values from Ref. 12: $c_l = 8.8$ and $c_t = 5.74$ *km/s* for alumina and $c_l = 4.8$ and $c_t = 3.3$ *km/s* for hafnia.

[33] W. S. Capinski, H. J. Maris, T. Ruf, M. Cardona, K. Ploog, and D. S. Katzer, Phys. Rev. B 59, 8105 (1999).

[34] S. Lee, D. G. Cahill and R. Venkatasubramanian, Appl. Phys. Lett. 70, 2957 (1997).

V. Publications related to program:

[1] N. T. Gabriel and J. J. Talghader, "Thermal conductivity and refractive index of hafnia-alumina nanolaminates," *Journal of Applied Physics*, vol. 110, 043526 (8 pages) , August 29, 2011.

[2] *Ph.D. Dissertation*, N. T. Gabriel, "High-power and high-aspect-ratio optical coatings by atomic layer deposition," University of Minnesota, February 2011. http://purl.umn.edu/131713

[3] N. T. Gabriel and J. J. Talghader, "Optical coatings in microscale channels by atomic layer deposition," *Applied Optics*, vol. 49, no. 8, pp.1242-1248, 2010.

VI. Interactions and Transitions:

During the program we had several interactions with organizations related to JTO's and ONR's development program in optical coatings.

1) We began an interaction with Anasys Corporation. Anasys is a company based in Santa Barbara, CA that specializes in manufacturing scientific equipment for measuring the relative thermal conductivities of nano-scale features using AFM technology. This interaction has subsequently led to a JTO program (FA9451-10-D-0224) to develop AFM-based infrared measurement tools for optical materials and coatings.

2) We had a collaboration to trade measurements on optical coatings with the Colorado State University research group of Prof. Carmen Menoni. CSU reproduced some basic measurements on our ALD films and oversaw the testing

of absorption (at Stanford University) and pulsed laser breakdown (at the University of New Mexico). We measured the thermal conductivity of their films.

3) Stanford University – (See above) Dr. Ashot Markosyan of Stanford measured the absorption of our ALD films using photothermal common path interferometry.

4) University of New Mexico – (See above) The research group of Prof. Wolfgang Rudolph measured the pulsed laser damage threshold of our ALD films.

VII. PhD Graduates:

Nicholas T. Gabriel
Electrical and Computer Engineering
University of Minnesota
February 2011
Advisor: Joseph J. Talghader

Ph.D. Dissertation, N. T. Gabriel, "High-power and high-aspect-ratio optical coatings by atomic layer deposition," University of Minnesota, February 2011. http://purl.umn.edu/131713